The Island Wind-Buoyancy Paradox

Agatha M. De Boer, Doron Nof*

Department of Oceanography, Florida State University,

Tallahassee, Florida

*To whom correspondence should be addressed; E-mail: nof@ocean.fsu.edu.

November 14, 2002

Abstract

In recent years, a variety of studies have suggested that the meridional overturning circulation is at least partially controlled by the Southern Ocean winds. The paradoxical implication is that a link exist between the surface buoyancy flux to the ocean (which is needed for the density transformation between surface and deep water) and the wind. These forcings have traditionally been viewed as independent drivers of the ocean circulation. Here, the paradox is formally stated in the framework of a gigantic island that lies between latitude bands free of continents (such as the land mass of the Americas).

The choice of such an island on a sphere was made because it enables one to obtain analytical solutions and it circumvents the need to calculate the torque exerted on zonal sills adjacent to the island tips (e.g., the Bering Strait). The torque calculation in notoriously difficult and is avoided here by the clockwise integration which goes twice through the western boundary of the island (in opposite directions) eliminating any unknown pressure torques. The derived wind-driven overturning is shown to be consistent with Godfrey's Island Rule when the rule is extended to include the sinking or upwelling adjacent to the island. In addition, the consideration of vertical exchange in the Island Rule eliminates the need to make the level-of-no-motion assumption.

The paradox is resolved qualitatively, using salinity and temperature mixed dynamical-box models and a temperature slab model, and quantitatively, employing a numerical model. We show that in all cases the ocean stratification and thermocline depth adjust themselves to allow the overturning imposed by the wind. The salinity and temperature box models suggest that stronger southern winds will tend to weaken the vertical and horizontal salinity stratification so that it is easier for the conversion of deep to surface water (and vice versa) to take place. A temperature slab model (i.e., y-dependent) offers a more detailed picture; stronger southern winds flatten the meridional temper-

ature profile and shift it northwards (so that it lags the atmospheric temperature).

The (process orientated) numerical model is adapted to include a thermodynamic parameterization for the surface heat and freshwater fluxes. In response to stronger southern winds, the thermocline thickens in the north, releases more heat to the atmosphere and, therefore, converts more surface to deep water.

1 Introduction

Traditionally the meridional overturning has been regarded as a large scale flow driven by temperature and salinity differences. Hence, the name thermohaline circulation. The gradients are set up by the surface heat and freshwater fluxes. In a groundbreaking study, Toggweiler and Samuels (1995) challenged this view by revealing a strong correlation between North Atlantic Deep Water (NADW) formation and winds over the Southern Ocean (SO). Since then, numerous models have corroborated this connection, albeit with varying sensitivity (McDermott 1996; Rahmstorf and England 1997; Bjornsson and Toggweiler 2001; Nof 2000; Nof 2002a; Nof 2002b; Klinger et al. 2002).

The importance of SO winds lies in the fact that they blow over a latitudinal belt of the ocean that is free of continents. Not only are the winds strong (due, partly, to the lack of surface topographic obstacles) but, more importantly, the open latitude belt ocean dynamics is fundamentally different from that of bounded ocean basins (Gill and Bryan 1971). A net geostrophic meridional flow is prevented by the open channel which encompasses the entire globe. Consequently, to conserve mass, an amount of water equal to the northward driven Ekman flow must either return through non-geostrophic eddy fluxes (Gnanadesikan 1999; Speer et al. 2000; Sloyan and Rintoul 2001), or sink below topography where it can return southward in geostrophic balance. A good overview of the relative importance of these two return pathways is provided by Rintoul et al. (2001). Some of the sinking may occur in the South Atlantic and South Pacific (Döös and Webb 1994), but presumably a significant portion sinks in the North Atlantic, where known regions of deep convection exist (Killworth 1983). It should be noted that it is not the southern Ekman water itself that crosses the equator and later sinks to the deep ocean, but rather the Sverdrup interior water (Nof and de Boer 2002).

In a recent article, Wunsch (2002) pointed out that the term "thermohaline circulation" is a misnomer because surface buoyancy fluxes cannot provide the energy needed to overturn a stratified ocean. He suggested to use instead the name "meridional overturning circulation" for the overturning of mass for which tidal and wind energy is required (rather that buoyancy flux). The inability of the heat and freshwater fluxes to overturn the ocean without additional energy is manifested in the "missing mixing" dilemma (Webb and Suginohara 2001).

In the conventional picture of the conveyer belt (Broecker 1987), the upwelling occurs through downward mixing of heat in low latitudes (Munk 1966), but observational evidence indicate that diapycnal mixing in the thermocline is insufficient to close the circulation budget (Ledwell et al. 1993). In the alternative scenario of an overturning driven by strong southern winds, the upwelling can occur in the SO through wind divergence. Toggweiler and Samuels (1998) found that such a wind-driven overturning circulation can exist without vertical mixing, provided that an Antarctic circumpolar channel is present. Furthermore, using a new tracer method, Döös and Coward (1997) found that most of the NADW upwells in the SO. Other related works that concern the SO winds are that of Gille (1997), Stevens and Ivchenko (1997), Tsujino and Suginohara (1999), Karsten et al. (2002), and Greatbatch and Lu (2002).

In section (2) we formally derive the meridional overturning associated with a gigantic island on a sphere (**Fig. 1**) using, what we will call the, "Belt Constraints". These are expressions for the transport across a latitudinal belt free of continents in terms of the zonal wind field at that latitude. In a stratified ocean, the resulting wind-driven overturning circulation necessitates surface heat and freshwater fluxes to facilitate buoyancy transition from deep water to surface water and vice versa. We point out the paradoxical link between the seemingly independent wind and thermodynamic surface forcings. In section (3) it is argued that a barotropic ocean of the above geometry (i.e., an island on a sphere), subject to the linearized momentum equations with dissipation limited to Western Boundary Currents, can never reach a steady state.

The one island is chosen to resemble, for example, the land mass of the America's (**Fig. 2**). A more realistic depiction would have been two large islands, where the second represents the Africa-Eurasia continents (Nof 2002a). Actually, any geometry, that leaves at least one open latitude band free of continents, will be subject to a wind-driven overturning and, therefore, reveal the paradox. Nevertheless, we prefer to address the case of one island because it is simple, can be dealt with analytically, and is sufficient to elucidate the paradox. In addition, it illustrates the necessity to include thermodynamics in the island rule (IR) for gigantic islands. The IR, first introduced by Godfrey (1989), offers an alternative method to derive the transport into and out of an basin to the east of an island. A variety of studies have examined and applied the IR to islands of intermediate size (see e.g., Pedlosky et al. 1997; Firing et al. 1999; Stanton 2001 and other earlier papers mentioned therein) but the first application to the continental landmasses of the Americas and Africa-Eurasia was done by Nof (2000,2002a). In section (4) the two methods of calculating the overturning circulation (i.e., the Belt Constraints and the IR) are shown to be consistent when a sinking term is included in the IR (to represent thermodynamic processes). In addition, the needlessness of the level-of-no-motion assumption for the new "Thermodynamic Island Rule" is discussed.

The reader will notice that the Americas and Asia are only divided by the shallow Bering Strait (45m deep). The sea-level is, of course, continuous across the strait no matter how shallow it is, so that a contour integration of the sea-level can always be done. The IR requires, however, a contour integration of the vertically integrated pressure (from the free surface to a fixed depth or a level-of-no-motion) rather than a contour integration of the sea-level, and this may be discontinuous across the strait due to a torque exerted on the sill (see ,Nof 2002a). This has been the main drawback of the Nof (2000, 2002a) gigantic island calculations.

In our present island derivation the sill is <u>inconsequential</u> because the integration path follows the western boundary of the island twice (but in opposite directions), and therefore, the unknown torque cancels itself at the strait (**Fig. 2**). Note that, for the earlier applications of the IR to the Americas (Nof 2000) and the Africa-Eurasia continents (Nof 2002a) the Bering Strait was traversed only once, so that the torque on the sill had to be considered.

The paradox is resolved by showing that the ocean stratification adjusts itself so that any buoyancy forcing is sufficient to allow the circulation imposed by the wind. In section (5) we show this conceptually with the use of a salinity and temperature box model and a temperature slab model. In section (6) a reduced gravity model, adapted to include buoyancy forcing, is used to resolve the paradox numerically. Our results are summarized in section (7)

2 The Belt Constraint and the paradox

Consider a single meridionally elongated island on a sphere (**Fig. 1**). The net north-south transport across the contours passing through the island tips can be derived analytically as follows. We integrate the linearized Boussinesq momentum equations for a continuously stratified fluid from the surface to a fixed depth, H, below the Ekman layer (so that the stress is zero) and above the bottom topography,

$$-\rho_o f V = -\frac{\partial P}{\partial x} + \tau^x, \quad (1)$$

$$\rho_o f U = -\frac{\partial P}{\partial y} + \tau^y - RV, \quad (2)$$

where ρ_o is the mean density, f the coriolis parameter and U and V are the depth integrated zonal and meridional velocity (respectively). P is the depth integrated pressure (from the surface to H, a predetermined depth which is not necessarily a level-of-no-motion) and τ^i is the surface wind stress in the i direction. Note that, for clarity, all variables are defined in both the text and the Appendix. Equations (1) and (2) correspond to a Sverdrup interior and frictional western boundary currents. Most of the energy dissipation occurs in the western boundary region through the term RV (where R is a frictional parameter). Integrating (1) zonally around an open latitude band free of continents, eliminates the pressure term so that,

$$Q_i = -\frac{\oint_i \tau^x dx}{\rho_o f_i}, \tag{3}$$

where Q_i is the transport across the integration path, i, from the surface to H. For the remainder of this paper we shall refer to (3), previously derived by Nof (2002b), as the "Belt Constraint". The amount of water that converges between the tips of the island in **Fig. 1** can now readily be derived from the Belt Constraint,

$$W = Q_1 - Q_2, \tag{4}$$

where the subscripts 1 and 2 refer to the southern and northern tips respectively. Steady state conditions require that an amount of water, W, sink below H and return to its origin. We shall assume adequate bottom topography at the latitude of the island tips to enable a return geostrophic flow at depth.

The wind, therefore, drives a meridional overturning that requires sinking and rising of water (to connect the opposing surface and deep flows). In a stratified ocean large vertical excursions are accompanied by buoyancy transformations. (Note that on smaller scales vertical exchange can occur along isopycnals.) The density changes are facilitated by surface heat and freshwater fluxes. Herein lies the paradox. Traditionally, wind and surface buoyancy fluxes have been regarded as independent forces, but the above example indicate that they must be aligned.

3 The spherical barotropic ocean with an island

Before proceeding to resolve the paradox, we shall briefly discuss the case of a barotropic ocean with a meridional island.We shall argue that a homogeneous ocean with the island geometry shown in **Fig. 1** and subject to the linearized momentum equation (1) and (2) can never reach a steady state. Analogous to the stratified ocean scenario, winds will converge water between the island tips and again, the water needs to sink and return at depth. Yet, unlike the baroclinic ocean, there is no means for the flow to change its direction and establish a subsequent southward return flow, so that a steady state cannot be reached.

To show this, let us first consider the interior ocean (away from the western boundary). Between the surface and bottom Ekman layers, the flow is governed by the geostrophic and hydrostatic equations which are,

$$\rho f v = -p_x, \qquad -\rho f u = -p_y, \tag{5}$$

$$p = -\rho g z + p'(x,y), \tag{6}$$

where ρ is the density, f the coriolis parameter, u and v the velocities in the x and y direction (respectively), g the gravitational constant, p the pressure, and p' the deviation from hydrostatic pressure from the pressure associated with a state of rest. Substituting (6) into (5) and taking the derivative with respect to z, yields the familiar Taylor-Proudman condition,

$$u_z = 0, \qquad v_z = 0. \tag{7}$$

implying that there cannot be a flow reversal in the interior.

A remaining question is whether there can be any reverse flow via the interior bottom Ekman layer. However, a scaling analysis indicates that the surface Ekman pumping is much stronger than that induced by bottom friction (see e.g.,Cushman-Roisin 1994, Page 114), so that the interior bottom layer is also unable to carry a flow of equal magnitude to the surface Ekman flow. The Western Boundary is the only remaining candidate which comes to mind. Yet, here, too, the flow away from the surface and bottom is independent of depth (see e.g.,Pedlosky 1987, Chap. 5). The bottom Ekman layer in the Western Boundary is indeed strong, but the direction of the flow is governed by the flow above it and not by the surface wind stress so that a reversal is not allowed here either. In conclusion, the water converged by the wind stress can not be returned by interior or bottom flows so that the barotropic ocean, subject to (1) and (2), will not be able to reach a steady state.

4 Thermodynamic Island Rule

So far we have introduced the Belt Constraint (3) for a flow across an open latitude band. This enabled us to determine the transport across a latitudinal contour barely touching the tips of a continental island. An alternative method for the derivation of the transport into (and out of) a basin to the east of an island is the IR of Godfrey (1989). The essence of the IR is an integration of the linearized momentum equations along a closed path that avoids the frictional western boundary region. The result is an expression of the circulation around the island in terms of the wind field along the path.

In this section we investigate the compatibility of the two Belt Constraints with the IR. We will show that, in order for the IR to be consistent with the Belt Constraints, thermodynamics must be included. We shall include the thermodynamics by allowing sinking east of the island. Our starting point is again the horizontal momentum equations. We integrate (1) along AB and CD (see **Fig. 3)** and (2) along BC and DA.

Adding the four resulting equations yields,

$$\rho_0(-f_1 Q_1 + f_2 Q_2) = \oint \tau^r \, dr, \tag{8}$$

where, again, the subscripts 1 and 2 refer to the southern and northern island tips so that $Q_{1,2}$ are the transports across AB and CD respectively. The integral $\oint \tau^r \, dr$ is the anti-clockwise integrated wind stress along the path. Because the frictional term RV is of O(1) only in the western boundary region (which we avoid in this integration), it does not enter the rest of the problem.

A preliminary word about the vertical integration limit is appropriate here. In the traditional IR it is assumed that no vertical exchange occurs between the upper and the lower layer east of the island, so that,

$$Q_1 = Q_2. \tag{9}$$

To justify this assumption the equations were originally integrated to a presupposed level-of-no-motion. We will not use this constraint and are, therefore, free to integrate to either a level-of-no-motion or to a fixed depth. This important issue will become clear shortly. The original island rule can be recovered from (8) and (9),

$$Q_1 = Q_2 = \frac{\oint \tau^r \, dr}{\rho_0(f_2 - f_1)}. \tag{10}$$

As mentioned, the original IR can be applied to a single meridional island on a sphere by choosing the integration path indicated in **Fig. 4.** The resulting transports (10) are clearly <u>inconsistent</u> with the transports derived from the Belt Constraint (3). This is, of course, because the original IR (10) does not account for the sinking that is required between the island tips. To resolve this, we include a term $W = Q_1 - Q_2$ to represent the vertical mass exchange between the upper and lower layer east of the island. In the framework of the original island rule, the boundary between the layers is the level-of-no-motion. Extension of the IR to allow thermodynamic processes through W allows us to integrate to a fixed depth.

Our "thermodynamic island rule" has richer dynamics than the original IR in the sense that it gives information about the vertical structure of the flow. In addition, the level-of-no-motion assumption, which is weak in higher latitudes is no longer needed. Furthermore, the assumption of $Q_1 = Q_2$ is far from true for gigantic islands such as the Americas. In fact, we have shown in section (2) that for an island whose tips extend to open latitudes, sinking east of the island is not merely likely, but essential. Solving for Q_1 and Q_2 in terms of W gives,

$$Q_1 = \frac{\oint \tau^r dr + f_2 W}{\rho_0 (f_2 - f_1)}, \tag{11}$$

$$Q_2 = \frac{\oint \tau^r dr + f_1 W}{\rho_0 (f_2 - f_1)}. \tag{12}$$

These transports do not resemble the Belt Constraint (3) at first glance, but substitution of (4) into (11) and (12) reveals that they are identical.

5 Conceptual models

We now proceed to resolve our paradox, i.e., we demonstrate that the ocean can always adjust its salinity and temperature field to accommodate the sinking imposed by the wind. To show this, we employ three conceptual analytical models. The first two are mixed dynamical-box models of temperature and salinity (respectively). With "mixed dynamical-box model" we mean that the thermodynamic properties of the boxes (i.e., S and T) are completely mixed, but that the transport between the boxes are determined dynamically. The third model is a temperature slab model of the upper ocean.

a. Salinity box model

The salt dynamical-box model consist of a ocean split into two boxes at the southern tip of an island in an open latitude band (**Fig. 5a**). To simplify the problem, we now take the northern tip of the island to lie at the North Pole so that a third box north of the island is redundant. The boxes are a conceptual analog for the oceans south and north of 55^{o}S, the latitude of Drake Passage. A net surface flow, Q, from the southern box to the northern box is determined by the wind and the Belt Constraint. We assume adequate bottom topography at this latitude to enable the return geostrophic flow at depth. On the basis of the observed freshwater fluxes in the ocean, the net surface freshwater flux, F_F, is taken to be positive for the southern box and equal but negative in the northern box (Wijffels et al. 1992). Conservation of salt for the southern box gives,

$$\frac{\partial(V_1 S_1)}{\partial t} = (Q - F_F)S_2 - QS_1, \tag{13}$$

where V is the volume of the box, t is the time, S is the salinity and the subscripts 1 and 2 refer to the southern and northern boxes respectively. We see that an increase in Q acts to make the Southern Ocean more salty and, similarly, the Northern Ocean becomes fresher. The salinity adjustment continues until a new steady state it reached, namely,

$$S_1 = (1 - \frac{F_F}{Q})S_2. \tag{14}$$

As the wind-driven transport increases, the salinity difference between the two boxes will merely decrease to accommodate the additional transport. In other words, a constant freshwater flux can convert more lower layer to upper layer water only when the salinity difference between the layers is reduced. In the real ocean, a weaker stratification would produce the same effect. Conversely, weaker Southern winds would intensify the stratification.

b. Temperature box model

The temperature field reacts somewhat differently to the winds. Not only does the stratification influence the ease of vertical exchange (as in the salinity case), but it also effects the heat exchange with the atmosphere. Again, we consider a simple box model of the ocean temperature (**Fig. 5b**). The heat flux, F_H, is taken to be proportional to the difference between the oceanic temperature, T and atmospheric temperature, $\widehat{T}$, so that $F_H = \lambda(\widehat{T} - T)$, where λ is a proportionality constant. This type of parameterization can be regarded as a bulk parameterization of latent and sensible heat loss or simply as a restoring boundary condition on the upper layer temperature, T (Rahmstorf and Willebrand 1995). For the southern box, the conservation of heat gives,

$$\frac{\partial T_1}{\partial t} = \frac{Q}{V_1}(T_2 - T_1) - \frac{\lambda}{C_p \rho H}(T_1 - \widehat{T}_1), \tag{15}$$

where C_p is the heat capacity of sea water, V_1 is the box volume, H the layer depth and ρ the average water density. The equation for the northern box is similar. For a steady state ocean (and atmosphere) the total heat flux (i.e., the sum of the heat fluxes into the two boxes) must be zero,

$$\lambda V_1(T_1 - \widehat{T}_1) + \lambda V_2(T_2 - \widehat{T}_2) = 0. \tag{16}$$

Assuming a steady state, we can now solve for T_1 and T_2 from (15) and (16),

$$T_{1,2} = \left[\left(\frac{\lambda V_{1,2}}{C_p \rho H Q} + \frac{V_{1,2}}{V_{2,1}}\right)\widehat{T}_{1,2} + \widehat{T}_{2,1}\right] / \left[1 + \frac{\lambda V_{1,2}}{C_p \rho H Q} + \frac{V_{1,2}}{V_{2,1}}\right]. \tag{17}$$

The solution of (17) for $\widehat{T}_1 = 5^oC$ and $\widehat{T}_2 = 15^oC$ is plotted as a function of Q in **Fig. 6**. To illustrate the effect of the box volumes, the southern box was chosen to be 5 times smaller than the northern box. As the transport increases, the oceanic temperature diverts from the atmospheric temperature. The smaller volume of the southern box renders it more vulnerable to the interbox transport. Similar to the salinity box model, the difference in the temperature between the two boxes shrinks in response to stronger southern winds. This is again analogous to a weakening of the oceanic stratification. A curious situation arises from our choice of atmospheric temperatures and transport direction. The surface flow from the southern box to the northern box is colder than the opposing deep flow, clearly an unstable stratification in a constant salinity ocean. In the real ocean, we expect that salinity will have a stabilizing effect, as the surface water in the south is fresher than the deep water (i.e., $S_1 < S_2$). In addition, the averaging of the box temperatures over a wide latitudinal range introduces unrealistic local temperatures. In other words, even if the deep water that sinks in the North Atlantic is near freezing, the overall mean temperature of the upper layer ocean north of 55^{o}S is much higher. This effect is eliminated in a y-dependent slab model of the upper ocean which is discussed in the next section.

c. Temperature slab model

Consider a slab of ocean (**Fig. 7**) whose temperature has explicit y (latitude) dependence . A constant flow passes through the slab at a velocity and flux determined by the wind. The water sinks in the northern hemisphere at 65^{o}N, flows southward in the deep ocean and is upwelled again at 55^{o}S. The southern boundary was chosen at the tip of South America and the northern boundary at the average latitude of North Atlantic deep convection (Killworth 1983). The surface water exchanges heat with the atmosphere according to $F_H = -\lambda(T - \widehat{T})$ while the deep ocean water conserves its temperature. We assume an atmospheric cosine temperature distribution of,

$\widehat{T} = \widehat{T}_m + \widehat{T}_0 \cos \frac{2y}{b}$, where b is the radius of the earth, $\widehat{T}_m$ is the average temperature and $\widehat{T}_0$ the amplitude of the variation around the mean (**Fig. 8**). Conservation of heat yields,

$$\frac{\partial T}{\partial t} = -v \frac{\partial T}{\partial y} - \frac{\lambda}{C_p \rho H}(T - \widehat{T}), \tag{18}$$

where v is the fixed meridional velocity of the flow through the slab (given by the wind). The analytical solution of (18) is,

$$T = \widehat{T}_m + \frac{a^2 \widehat{T}_o}{a^2 + d^2 v^2} \cos dy + \frac{a d \widehat{T}_0 v}{a^2 + d^2 v^2} \sin dy + A e^{-\frac{ay}{v}}, \tag{19}$$

where $a = \lambda/(C_p \rho H)$, $d = 2/r$ and A is an integration constant to be determined. We solve for A by recognizing that, to conserve heat in the ocean, the incoming and outgoing temperatures must be equal. The final analytical solution is straightforward and is depicted in **Fig. 8** for two different velocities, $v = 1\, cm/s$ and $v = 10\, cm/s$.

Without any meridional transport, the ocean adopts the temperature profile of the atmosphere as its own temperature field. As the velocity (and, hence, the transport) is increased, the oceanic solution shifts northward, away from the atmospheric temperature profile. The north-south asymmetry produces a net northwards heat transport across the equator. In addition to the shift between the temperature peaks of the ocean and atmosphere, stronger velocities tend to flatten the oceanic temperature profile. This is again akin to a weaker stratification. It should be noted that, in reality, the atmospheric profile is also dependent on the oceanic temperatures. This would add another feedback which is presently neglected.

6 Numerical simulations

In this section we confirm our earlier analytical results numerically, i.e., using process oriented numerical simulations we show that the ocean will adjust itself to allow the overturning forced by the Southern winds. The model we use is a simple reduced gravity model that has been derived from the isopycnal model originally developed by Bleck and Boudra (1981,1986). We include a thermodynamic parameterization (details described below) and then perform 6 runs of increasing southern wind stress to test the overturning's response.

a. Model Description

The process-orientated model is a layer-and-a-half model, which means that the lower layer is assumed to be infinitely deep and at rest. A dynamic upper layer is governed by the continuity equation and the non-linear frictional momentum equations,

$$\frac{\partial u}{\partial t} + u\frac{\partial u}{\partial x} + v\frac{\partial u}{\partial y} - (f_0 + \beta y)v = -g'\frac{\partial h}{\partial x} + \frac{\nu}{h}\nabla \cdot (h\nabla u)\frac{\tau^x}{\rho h} - Ku, \qquad (20)$$

$$\frac{\partial v}{\partial t} + u\frac{\partial v}{\partial x} + v\frac{\partial v}{\partial y} + (f_0 + \beta y)u = -g'\frac{\partial h}{\partial y} + \frac{\nu}{h}\nabla \cdot (h\nabla v)\frac{\tau^y}{\rho h} - Kv, \qquad (21)$$

where u and v are the zonal and meridional velocities, f_o is the reference coriolis parameter, β is the derivative of the coriolis parameter with respect to y, g' is the reduced gravity, h is the upper layer thickness, ν is the viscosity, K is the linear drag coefficient and τ^x and τ^y are the zonal and meridional wind stresses. The equations are solved using an Arakawa C-grid (Arakawa 1966) finite difference expansion and the leap-frog scheme to advance in time. The model domain is a rectangle extending from 68^{o}S to 68^{o}N and covering 9000 km in the zonal direction. A thin meridional island lies between 53^{o}S and 65^{o}N (**Fig. 9a**).

Following Nof (2000, 2002a, 2002b), we made our runs more economical by reducing the gridpoints in the x and y direction by 15 and increasing the wind stress and beta correspondingly. These modifications lead to a reduction in the grid count (and consequently, the run time) by a factor of 15^2. The downside of the above modifications is an unnaturally large ratio between the eddies' size and the basin's size. This is not a problem in our runs because the eddies do not play a major role in the meridional mass exchange. Furthermore, this unnatural eddy-basin-ratio issue can be easily resolved by using a very large horizontal eddy viscosity coefficient that eliminates any long-lived eddies such as Gulf Stream rings. This essentially implies that our model is not an eddy-resolving model. Note also that, with our chosen parameters, the ratio between the Munk layer thickness $(\nu/\beta)^3$ and the basin size was still very small (as required) because our β was magnified.

Winds are adapted from the zonally averaged Hellerman and Rosenstein (1983) dataset. For the six different runs the wind stress south of the island is magnified by factors ranging from 0 to 3 (**Fig. 9b**). The runs are summarized in table 1.

b. Thermodynamic Forcing

Recall that, in a reduced gravity model the density of the upper layer is constant, so that buoyancy fluxes that would induce a density increase (decrease) in the upper layer can only be represented by a decrease (increase) of the upper layer thickness. This translates to a vertical velocity, w, in the continuity equation,

$$\frac{\partial h}{\partial t} + \frac{\partial (hu)}{\partial x} + \frac{\partial (hv)}{\partial y} = w = w_F + w_H, \tag{22}$$

where w_F is the contribution from the freshwater flux and w_H from the heat flux. The parameterization of w_F is straightforward. We assume a zonally independent distribution that varies in y according to a cosine function,

$$w_F = w_{Fo} \cos \frac{2\pi y}{68}, \tag{23}$$

where w_{Fo} is the amplitude of the function (**Fig. 9c**). Positive peaks, representing high precipitation regions are at the equator and the poleward boundaries. Evaporative regions peak at the sub-tropics.

Our heat flux parameterization is similar to that used by Cushman-Roisin (1987) in a two layer analytical model and by Spall (2002) in a numerical reduced gravity model. The heat buoyancy flux w_H is assumed to be proportional to the difference between the oceanic and atmospheric temperature. As mentioned earlier, this type of parameterization can be regarded as a bulk parameterization of latent and sensible heat loss or simply as a restoring boundary condition on the upper layer temperature, T (Rahmstorf and Willebrand 1995). In the absence of an explicit temperature variable, the upper layer thickness, h, is used as a proxy for T. The motivation for this choice lies in the fact that in a reduced gravity model (which, by definition, has a constant upper layer density) Δh is proportional to ΔT. The atmospheric temperature, $\widehat{T}$, is likewise converted to length dimensions, $\widehat{h}$, so that the vertical velocity is,

$$w_H = -\alpha(h - \widehat{h}), \tag{24}$$

where α is a proportionality constant. We chose α=2 x 10^{-6} s^{-1} so that an average $(h - \widehat{h})$ of 100m in the Southern Ocean would produce a source of 15 Sv (1 Sv = $10^6 m^3 s^{-1}$). Our parameterization differs from that of Cushman-Roisin (1987) and Spall (2002) in that they assumed a constant $\widehat{h}$, whereas we take $\widehat{h}$ as a cosine function of y,

$$\widehat{h} = \widehat{h}_m + \widehat{h}_o \cos \frac{2\pi y}{136}, \tag{25}$$

where $\widehat{h}_m$ is the mean and $\widehat{h}_o$ is the amplitude of the function. The atmospheric "temperature" peaks at the equator and decreases towards to poles. However, the heat flux distribution does not resemble the atmospheric temperature profile closely because it also depends on the thickness of the upper layer. The profile of the heat flux for the run where the wind amplification factor was one is depicted in **Fig. 9c**.

c. Weaknesses

Before continuing to describe our results, it is appropriate to discuss the main weaknesses of the model:

1) The use of the upper layer thickness as a proxy for the temperature is obviously potentially problematic. It is motivated by the following logic. For the density of the layer to remain constant while it is receiving heat from the atmosphere, h will have to increase in lieu of T. In other words, the heat is used to transform lower layer water to upper layer water instantly. However, in the real ocean, the heat from the atmosphere is not necessarily used locally for water mass conversion and, in that sense, our model misrepresents the ocean.

2) The heat flux is assumed to be proportional to the upper layer thickness (used as a proxy for the temperature). This is also potentially problematic because processes such as the freshwater flux and divergence of the flow field also effect h. These processes are, therefore, artificial components of our heat flux.

3) The conversion of the atmospheric temperature profile to ocean thickness units cannot be done rigorously. The choices of the atmospheric depth profile and heat flux proportionality constant was, therefore, somewhat arbitrary. As mentioned, we chose α=2 x 10^{-6} s^{-1} so that an average $(h - \widehat{h})$ of 100m in the Southern Ocean would produce a source of 15 Sv. Doubling or halving of this value changes our results (which is the transport across 55^oS) by less than 10%.

4) The freshwater flux parameter, w_{Fo}=2 x 10^{-4} m s^{-1}, was chosen along similar

lines. It results in a source of 7 Sv in the Southern Ocean. As in the case of the heat flux parameter, doubling or halving of w_{Fo} effects our results by less than 10%.

5) There is no feedback between the oceanic and the atmospheric temperature. In reality, the temperature of the atmosphere is not fixed, but rather, tends to follow the oceanic profile.

Overall, our buoyancy flux parameterization is not ideal. Yet it offers a compromise between a more complicated multi-layered ocean general circulation model and a simple reduced gravity model without any thermodynamics. The former is computationally expensive to use as a process-orientated tool and, more importantly, very difficult to interpret, while the latter is for obvious reasons not adequate for our analysis. Our middle of the way choice seem to be the best tool to use.

d. Results

As mentioned, six runs (for which the southern wind stress was amplified by a factor of 0 to 3) were executed. The velocity vectors and thickness contours for an amplification factor of 1 are shown in **Fig. 10**. The main features are two sub-tropical gyres sandwiching the equator, a sub-polar gyre in the north, and strong zonal flows in the Southern Ocean. For each run, the integrated transport across the 55^oS latitude was computed. In **Fig. 11** the results are compared to the theoretical transport given by the Belt Constraint (3). We see that the flow across the open latitude band follows very closely the increase in the wind stress at that latitude. The difference is due to lateral friction, linear drag and advection in the model (**Fig. 12**). Even though a circumpolar current forms, the friction associated with the current at the island tip is negligible. The model adapts to stronger winds by decreasing its upper layer thickness (equivalent to cooling) in the south and increasing it in the north. As a result, heat loss to the atmosphere in the Southern Ocean is reduced, the net buoyancy flux (freshwater plus heat) becomes more positive and, hence, more deep water is upwelled. In the north, the deeper upper layer (or thermocline) loses more heat to the atmosphere so that sinking is enhanced. This response was also found by Bjornsson and Toggweiler (2001) in a multi-layered ocean model coupled to a atmospheric energy balance model. Conversely, weaker winds result in a warmer southern ocean and cooler northern ocean.

7 Summary and discussion

In the last decade several studies have found a link between the global overturning circulation and the southern winds. The controversial implication of such a link is that the seemingly independent wind and buoyancy forcings must be coupled. We derived here the paradox formally in the framework of a meridional island (on a sphere) that lies between latitudinal bands free of continents.

We chose the single meridional island on a sphere problem (as representing the Americas) because it is sufficient to illustrate the paradox, enables one to obtain analytical solutions and avoids the notorious problem of computing the torque on the Bering Strait sill. The elimination of the torque issue is due to the fact that an integration around an island on a sphere goes through the western boundary and the strait twice (and in opposite directions) so that the torque is canceled out. The circulation associated with a two island system (i.e., the distribution of sinking between the two basins and the interbasin transport) will be addressed later and reported elsewhere.

At the island tips, the meridional transport is given by the Belt Constraint (3), which is a zonally integrated version of the linearized x-momentum equation. In essence the Belt Constraint requires that the northward transport above the topography be equal to the Ekman transport because the net geostrophic transport is zero. Eddy fluxes were neglected in the analysis, as it is not clear how large their contribution is, how they will respond to the wind and how to include them. The difference between the

Belt Constraints at the two island tips yields the amount of water that needs to sink (or rise) through the upper layer adjacent to the island. We derived a thermodynamic version of Godfrey's IR by including the sinking (or rising) in the basin east of the island (11,12) and showed that it is consistent with the Belt Constraints (3). The inclusion of vertical exchange in the island's eastern basin eliminates the need for the level-of-no-motion assumption which is made in previous IR calculations.

The paradox was resolved qualitatively, using two mixed dynamical-box models (**Fig. 5**) and a slab model (**Fig. 7**), and quantitatively with the aid of a numerical reduced gravity model (**Fig. 9**). The three conceptual models all carry a northward surface transport that is forced by the wind field and the Belt Constraint. The adjustment of the salinity field in the first box model to stronger southern winds is readily understood. Following an increase in the wind stress, additional conversion of water between the boxes is enabled by a reduction in the salinity difference between the boxes. In reality, vertical isohalines (such as the division between the boxes) do not exist. Rather, the boxes should be regarded partly as southern and northern boxes, and partly as upper layer and deep ocean boxes. The reduction in the salinity difference is, therefore, analogous to a weakening of both the horizontal and vertical stratification in the real ocean.

Likewise, the temperature field of the box model adjusts to the wind field, although the reaction is complicated by the feedback of the temperature on the surface heat flux. An increase in Southern winds tends to reduce the temperature difference between the boxes so that, again, the stratification is weakened (**Fig. 6**). A slab ocean model (which is y-dependent) was used to give a richer picture of the influence of the wind on the meridional temperature distribution. It was found that, for very weak winds (small meridional transport), the ocean temperature equilibrates with the atmosphere. Stronger winds have two effects. First, they shift the temperature profile northwards (so that it lags the atmospheric profile) and, second, the amplitude of the variations around the mean is reduced (**Fig. 8**). This is akin to a weaker stratification in the real ocean. Note that the northward heat transport is not necessarily increased or decreased by stronger winds because of the opposing effects of higher transport and weaker stratification.

The paradox was resolved quantitatively using a reduced gravity numerical model. Buoyancy forcing was included by adding a mass flux term in the continuity equation. The term consists of a variable heat flux contribution and a freshwater flux contribution that is fixed in time but has y-dependence. The heat flux is proportional to the difference between the upper layer temperature (approximated by the upper layer thickness) and an atmospheric temperature (converted to thickness units). The numerical model domain is a periodic ocean that contains only one long meridional island. A series of runs were performed where the southern winds were increased by a factor ranging from 0 to 3. The transport across the latitude of the southern island tip (**Fig. 9c**) was calculated and an excellent agreement was found with the Belt Constraint (3). As the winds increased, the thermocline in the north deepened ("warmed") and shallowed ("cooled") in the south. Note that the numerical model, having only one layer and a fixed reduced density, lacks the ability to resolve the effect of weaker stratification on the sinking (seen in the box models). Instead, it makes use of the feedback of the ocean temperature on the surface heat flux to accommodate the required sinking.

In view of our theoretical and numerical results, we conclude that the coupling between the wind and the surface buoyancy forcing occurs through an adjustment in the ocean stratification. As a response to stronger winds, both the temperature and salinity fields becomes more weakly stratified and, in addition, the thermocline deepens in the north.

Acknowledgments. This study was supported by the National Aeronautics and Space

Administration under grants NAG5-7630 and NGT5-30164; National Science Foundation contract OCE 9911324; and Office of Naval Research grant N00014-01-0291.

APPENDIX

List of Symbols

a	Constant, $a = \lambda/(C_p \rho_o H)$
A	Integration constant for slab model
b	Radius of the earth
C_p	Heat capacity of sea water
d	Constant, $d = 2/b$
f_0	Reference coriolis parameter in numerical model
f	Coriolis parameter
$f_{1,2}$	Coriolis parameters along the southern and northern island tips (Fig. 3)
g'	reduced gravity
h	Upper layer thickness in numerical model
$\widehat{h}$	Proxy for atmospheric temperature in depth units
$\widehat{h}_m$	Mean of $\widehat{h}$
$\widehat{h}_0$	Amplitude of the variation in $\widehat{h}$
H	Depth of box and slab model
K	Linear drag coefficient
P	Vertically integrated pressure
Q	Transport between southern and northern box (Fig. 5)
$Q_{1,2}$	Transports across the latitudes of the southern and northern island tips (Fig. 1)
r	Integration path
R	Interfacial friction coefficient
$S_{1,2}$	Salinities in the southern and northern boxes (Fig. 5)
T	Temperature of slab model (Fig. 7)

$\widehat{T}$	Atmospheric temperature in slab model (Fig. 7)
$\widehat{T}_m$	Mean atmospheric temperature in slab model (Fig. 7)
$\widehat{T}_0$	Variation of atmospheric temperature in slab model (Fig. 7)
$T_{1,2}$	Temperatures in the southern and northern boxes (Fig. 5)
u, v, w	Velocities in the x,y, and z directions
U, V	Vertically integrated transports in the x and y direction
$V_{1,2}$	Volumes of the southern and northern boxes (Fig. 5)
$w_{F,H}$	Vertical velocities associated with freshwater and heat fluxes
w_{Fo}	Amplitude of variation in w_F
W	Net sink of water adjacent to the island
α	Proportionality constant for heat flux, $w_H = -\alpha(h - \widehat{h})$
β	Variation of the coriolis parameter with y
λ	Proportionality constant for surface heat flux
ν	Viscosity
ρ_0	Average density
τ^r	Wind stress along the integration path r
$\tau^{x,y}$	Wind stress in the x and y direction

References

Arakawa, A. (1966). Computational design for long-term numerical integration of the equations of fluid motion. two dimensional incompressible flow. part I. *J. Comput. Phys. 1*, 119–143.

Bjornsson, H. and J. R. Toggweiler (2001). The climatic influence of Drake Passage. In D. Seidov, B. J. Haupt, and M. Maslin (Eds.), *The Oceans and Rapid Climate Change: Past, Present, and Future*, Volume Geophysical Monograph 126, pp. 243–259. American Geophysical Union.

Bleck, R. and D. Boudra (1981). Initial testing of a numerical ocean circilation model using a hybrid, quasi-isopycnic vertical coordinate. *J. Phys. Oceanogr. 11*, 755–770.

Bleck, R. and D. Boudra (1986). Wind-driven spin-up in eddy-resolving ocean models formulated in isopycnic and isobaric coordinates. *J. Geophys. Res. 91*, 7611–7621.

Broecker, W. S. (1987). The biggest chill. *Nat. Hist. 10*, 74–82.

Cushman-Roisin, B. (1987). On the role of heat flux in the Gulf Stream-Sargasso Sea subtropical gyre system. *J. Phys. Oceanogr. 17*, 2189–2202.

Cushman-Roisin, B. (1994). *Introduction to Geophysical Fluid Dynamics*, Chapter 8. Prentice Hall.

Döös, K. and A. Coward (1997). The Southern Ocean as the major upwelling zone of North Atlantic deep water. *WOCE Newsletter 27*, 3–17.

Döös, K. and D. J. Webb (1994). The Deacon cell and the other meridional cells of the Southern Ocean. *J. Phys. Oceanogr. 24*, 429–442.

Firing, E., B. Qiu, and W. Miao (1999). Time-dependent island rule and its application to the time-varying North Hawaiian ridge current. *J. Phys. Oceanogr. 29*, 2671–2688.

Gill, A. E. and K. Bryan (1971). Effects of geometry on the circulation of a three-dimensional southern-hemisphere ocean model. *Deep-Sea Res. 18*, 685–721.

Gille, S. (1997). The southern ocean momentum balance: Evidence for topographic effects from numerical model output and altimetry data. *J. Phys. Oceanogr. 27*, 2219–2232.

Gnanadesikan, A. (1999). A simple predictive model for the structure of the oceanic pycnocline. *Science 283*(5410), 2077–2079.

Godfrey, J. S. (1989). A sverdrup model of the depth-intergrated flow for the ocean allowing for island circulations. *Geophys. Astrophys. Fluid Dyn. 45*, 89–112.

Greatbatch, R. J. and J. Lu (2002). On the inconsistency between the Stommel box model and the Stommel-Arons model: A possible role for southern hemisphere wind forcing. Submitted to J. Phys. Oceanogr.

Hellerman, S. and M. Rosenstein (1983). Normal monthly wind stress over the world ocean with error estimates. *J. Phys. Oceanogr. 13*(7), 1093–1104.

Karsten, R., H. Jones, and J. Marshall (2002). The role of eddy transfer in setting the stratification and transport of a circumpolar current. *J. Phys. Oceanogr. 32*, 39–54.

Killworth, P. D. (1983). Deep convection in the world ocean. *Review of Geophysics and Space Physics 21*(1), 1–26.

Klinger, B. A., S. Drijfhout, J. Marotzke, and J. R. Scott (2002). Sensitivity of basin-wide meridional overturning to diapycnal diffision and remote wind forcing in an idealized Atlantic-Southern Ocean geometry. In press in J. Phys. Oceanogr.

Ledwell, J. R., A. J. Watson, and C. S. Law (1993). Evidence for slow mixing across the pycnocline from an open-ocean tracer-release experiment. *Nature 364*, 701–703.

McDermott, D. A. (1996). The regulation of northern overturning by southern winds. *J. Phys. Oceanogr. 26*, 1234–1255.

Munk, W. H. (1966). Abyssal recipes. *Deep-Sea Res. 13*, 707–730.

Nof, D. (2000). Does the wind control the import and export of the South Atlantic. *J. Phys. Oceanogr. 30*(11), 2650–2667.

Nof, D. (2002a). Is there a meridional overturning cell in the Pacific and Indian Oceans. *J. Phys. Oceanogr. 32*(6), 1947–1959.

Nof, D. (2002b). The Southern Ocean's grip on the northward meridional flow. Prog. Oceanogr., in press.

Nof, D. and A. M. de Boer (2002). From the Southern Ocean to the North Atlantic in the Ekman layer? Submitted to Bull. Amer. Meteor. Soc.

Pedlosky, J. (1987). *Geophysical Fluid Dynamics*, Chapter 5. Springer.

Pedlosky, J., L. J. Pratt, M. A. Spall, and K. R. Helfrich (1997). Circulation around islands and ridges. *J. Mar. Res. 55*, 1199–1251.

Rahmstorf, S. and M. H. England (1997). Influence of southern hemispheric winds on North Atlantic Deep Water flow. *J. Phys. Oceanogr. 27*, 2040–2054.

Rahmstorf, S. and J. Willebrand (1995). The role of temperature feedback in stabilizing the thermohaline circulation. *J. Phys. Oceanogr. 25*, 787–805.

Rintoul, S. R., C. W. Hughes, and D. Olbers (2001). The Antarctic Circumpolar Current System. In G. Siedler, J. Church, and J. Gould (Eds.), *Ocean Circulation and Climate*, pp. 271–302. Academic Press.

Sloyan, B. M. and S. R. Rintoul (2001). The Southern Ocean limb of the global overturning circulation. *J. Phys. Oceanogr. 31*, 143–173.

Spall, M. A. (2002). Wind- and buoyancy-forced upper ocean circulation in two-strait marginal seas with application to the Japan / East Sea. *J. Geophys.*

Res. 107(C1), 6.1–6.12.

Speer, K., S. R. Rintoul, and B. Sloyan (2000). The diabatic deacon cell. *J. Phys. Oceanogr. 30*, 3212–3222.

Stanton, B. R. (2001). Estimating the East Auckland Current transport from model winds and the island rule. *N. Z. J. Mar. and Freshwater Res. 35*(3), 531–540.

Stevens, D. P. and V. O. Ivchenko (1997). The zonal momentum balance in an eddy resolving general-circulation model of the Southern Ocean. *Quart. J. Roy. Meteor. Soc. 123*, 929–951.

Toggweiler, J. R. and B. Samuels (1995). Effect of Drake Passage in the global thermohaline circulation. *Deep-Sea Res. 42*(4), 477–500.

Toggweiler, J. R. and B. Samuels (1998). On the ocean's large-scale circulation near the limit of no vertical mixing. *J. Phys. Oceanogr. 28*(9), 1832–1852.

Tsujino, H. and N. Suginohara (1999). Thermohaline circulation enhanced by wind forcing. *J. Phys. Oceanogr. 29*, 1506–1516.

Webb, D. J. and N. Suginohara (2001). The interior circulation of the ocean. In G. Siedler, J. Church, and J. Gould (Eds.), *Ocean Circulation and Climate*, pp. 205–214. Academic Press.

Wijffels, S. E., R. W. Schmitt, H. L. Bryden, and A. Stigebrandt (1992). Transport of freshwater by the oceans. *J. Phys. Oceanogr. 22*(2), 155–162.

Wunsch, C. (2002). What is the thermohaline circulation? *Science 298*(5596), 1179–1181.

List of Tables

List of Figures

Exp. no.	1	2	3	4	5	6
Wind amp. factor	0	0.1	1	1.5	2	3

Table 1: The six experiments. Common model parameters are Δx=15 km, Δy=15 km, Δt=360 s, g'=0.015 m s^{-2}, H=800 m, β=3.4 x 10^{-10} m^{-1} s^{-1}, ν=1600 m^2 s^{-2}, K=2 x 10^{-6} s^{-1}, α=2 x 10^{-6} s^{-1}, $\widehat{h}_m$=800 m, $\widehat{h}_0$=100 m, w_{Fo}=2 x 10^{-4} m s^{-1}

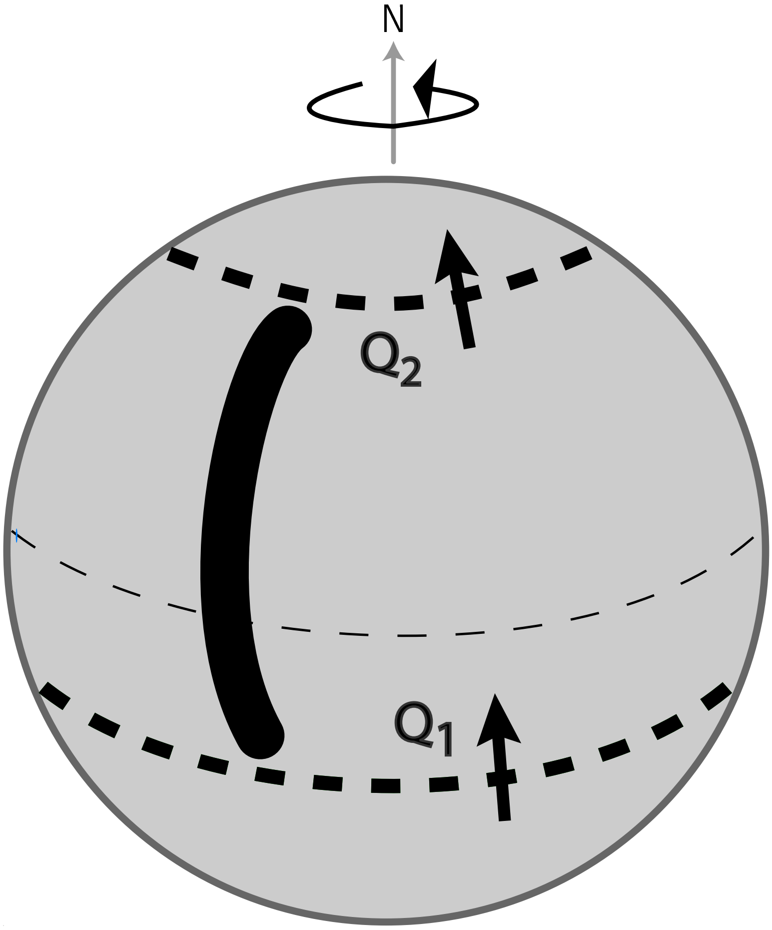

Fig 1: A single meridional island on a sphere. $Q_{1,2}$ are the wind-forced transports (in the upper layer, above topography) across the southern and northern belt, respectively. For $Q_1 - Q_2 > 0$ there must be a net sink between the island tips. The island represents the Americas or the Africa-Eurasia continents.

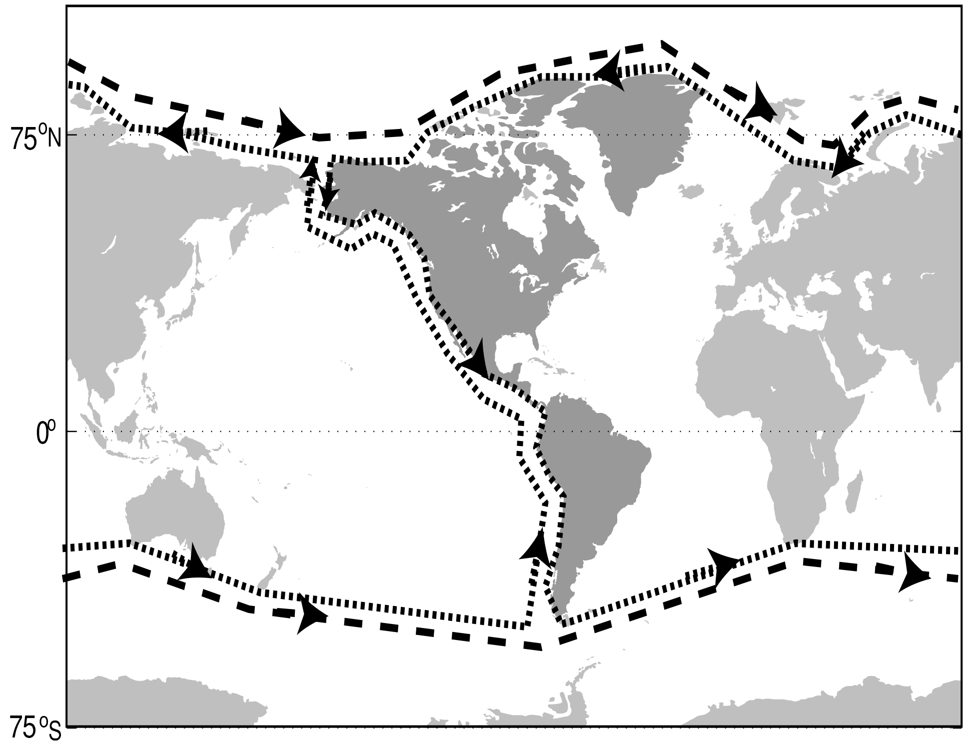

Fig 2: The continents of the Americas are chosen here to illustrate the IR for a gigantic island on a sphere. The dotted line is the wind integration contour for the IR and the dashed lines are the contours used for the belt constraints. Because the Americas are chosen to resemble a single island on a sphere, the integration path does not follow the eastern boundary of Africa and Europe (as in Nof 2002). Note that, even though the Bering Strait is only 50m deep, the sections of the IR integration path along the eastern boundary of the Americas cancel so that the pressure drop across the strait is irrelevant.

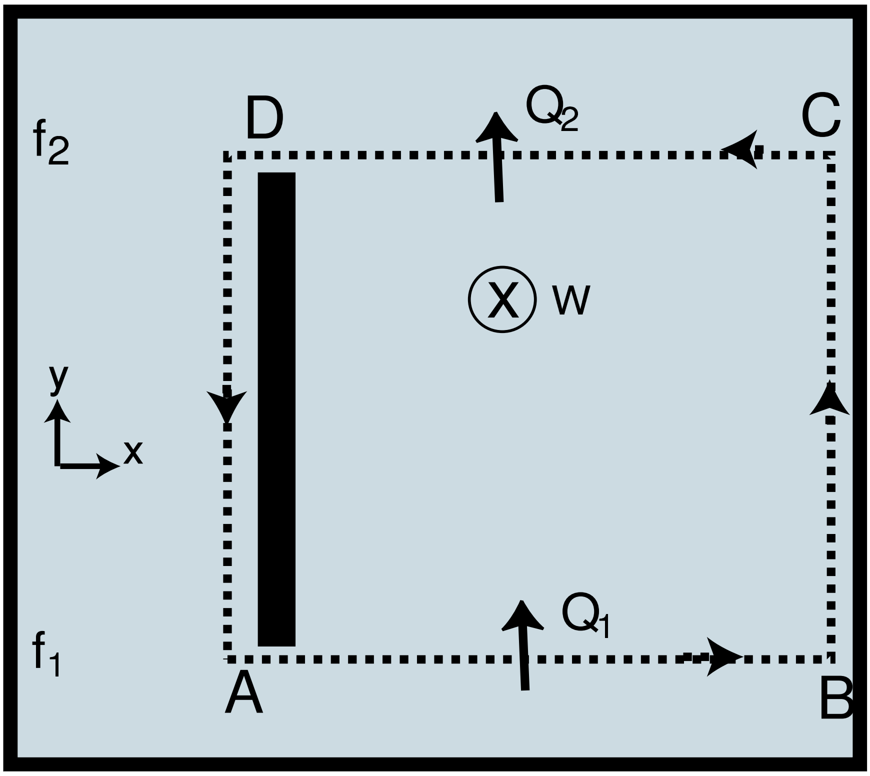

Fig 3: The top view of an island in a closed ocean basin. The island rule is derived from an integration of the momentum equations along the dashed contour, ABCDA. $Q_{1,2}$ are the transports across AB and CD respectively and $f_{1,2}$ are the coriolis parameters at the island tips. Downwelling, W, is indicated by $\otimes$.

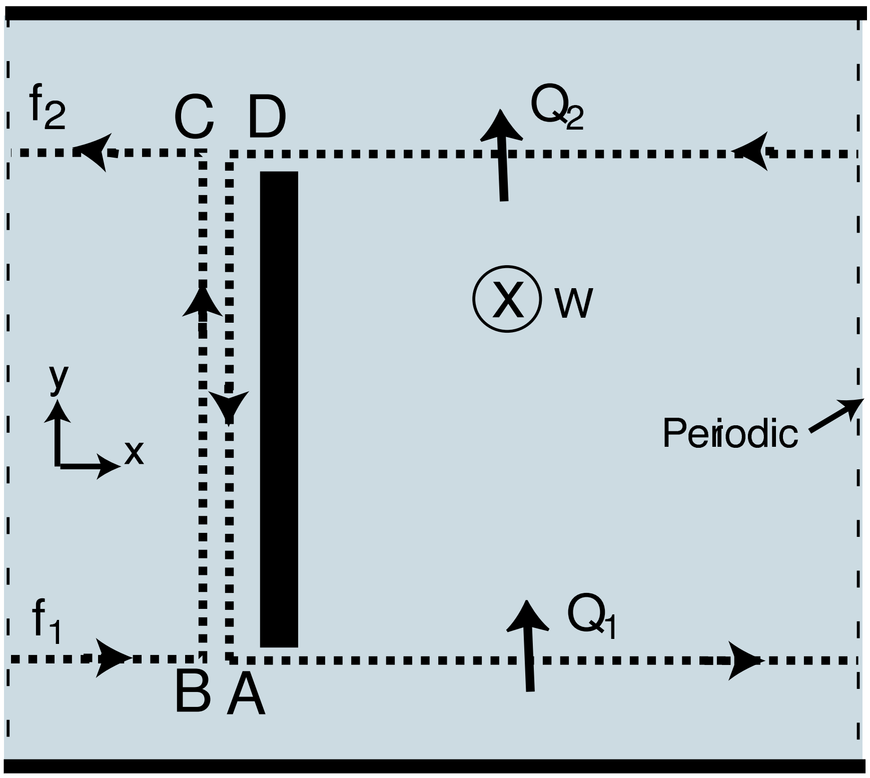

Fig 4: Top view of a zonally periodic ocean basin. The thick dashed contour shows the integration path (ABCDA) for an island on a sphere. It differs from **Fig. 3** in that, apart form the island itself, there are no other eastern boundaries. The thin dashed line indicates the periodic boundaries. Again, $Q_{1,2}$ are the transports across AB and CD respectively and $f_{1,2}$ are the coriolis parameters at the island tips. Downwelling, W, is indicated by $\otimes$.

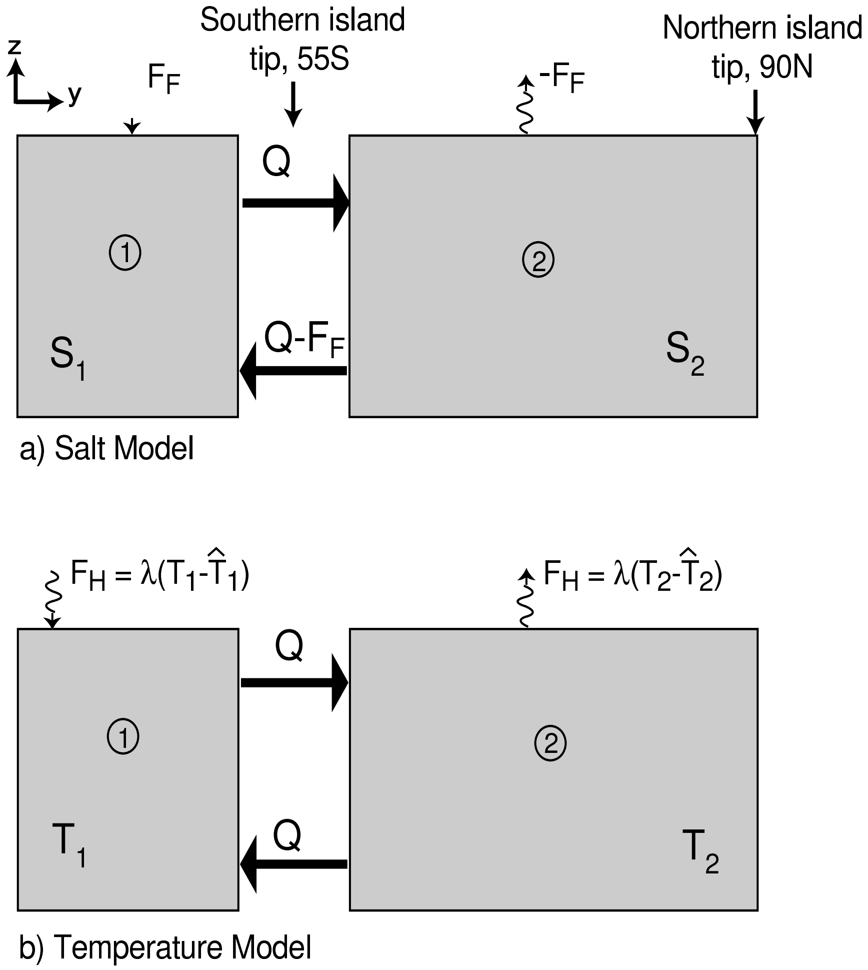

Fig 5: Two box models of a) salinity (S) and b) temperature (T). The southern and northern boxes (1 and 2, respectively) are divided at the southern tip of an island (eg., the Americas) and lies in a latitude belt free of continents. For simplicity, the island is taken to extend to the North Pole, so that an additional third northern box is redundant. The surface transport between the boxes, Q, is determined by the Belt Constraint (eq. 3) and the zonal wind stress at the division. A return flow at depth closes the mass budget. The salinity boxes exchange freshwater, F_F, with the atmosphere. F_F is positive into the southern box and equal but negative into the northern box (Wijffels et al. 1992). The temperature boxes exchange heat, F_H with the atmosphere in an amount proportional to the difference between T and the atmospheric temperature, $\widehat{T}$. For clarity, the salinity and temperature models are shown separately, but the processes (T and S adjustments) are mutually independent and could have be presented simultaneously.

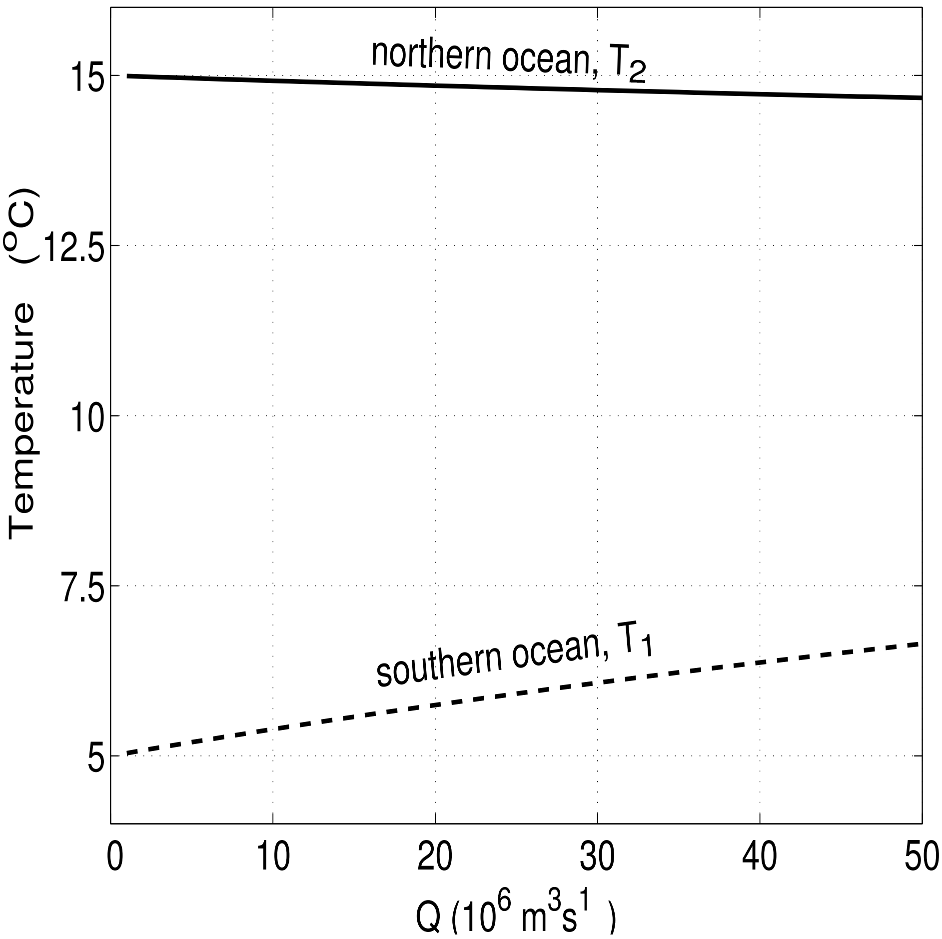

Fig 6: The temperature of the oceanic box model as a function of the transport (Q) between the boxes (17). The solid line shows the temperature of the northern box and the dashed line of the southern box. Atmospheric temperatures were taken to be $\widehat{T_1} = 5^oC$ and $\widehat{T_2} = 15^oC$. As the transport increases, the oceanic temperature diverts from that of the overlying atmosphere and the temperature difference between the boxes decreases. Therefore, as in the salinity model, the stratification weakens as the winds are increased. The southern ocean is more strongly effected by the transport than the northern ocean because we took its volume to be 5 times smaller. The parameters are $V_1 = 10^{16}m^3$, V_2= 5. $10^{16}m^3$, λ=50 Wm$^{-2}K^{-1}$, ρ=1000 Kgm^{-3}, C_p=4000 JKg$^{-1}K^{-1}$, H= 500 m.

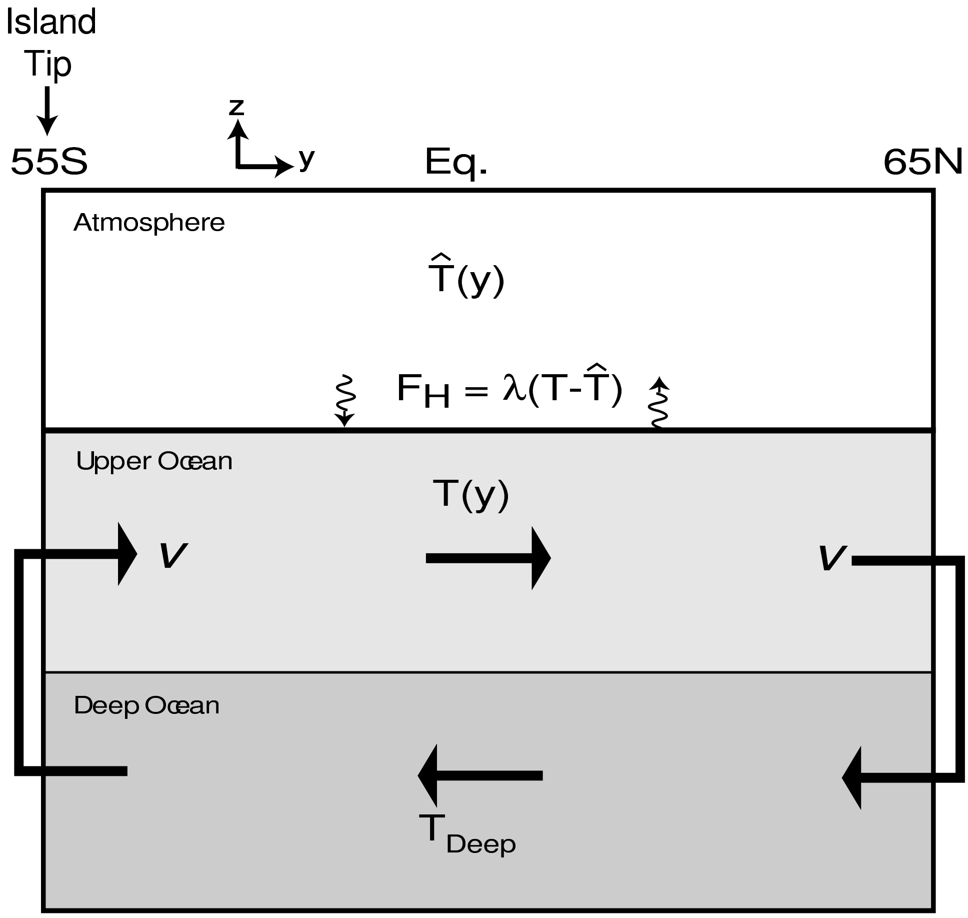

Fig 7: Slab model of the ocean and atmosphere from 55S to 65N. The upper layer presents the atmosphere which has a fixed y-dependent temperature profile, $\widehat{T}(y)$, depicted in **Fig. 8.** Below the atmosphere lies the upper ocean which exchanges heat with the atmosphere proportional to $(T - \widehat{T}(y))$. A constant flow of water flows northward in this layer at a constant velocity, v, determined by the Belt Constraint (3) and the zonal wind stress at 55^oS. North of 65^oN the water is subducted to the deep layer, returns south, and is upwelled again south of 55^oS

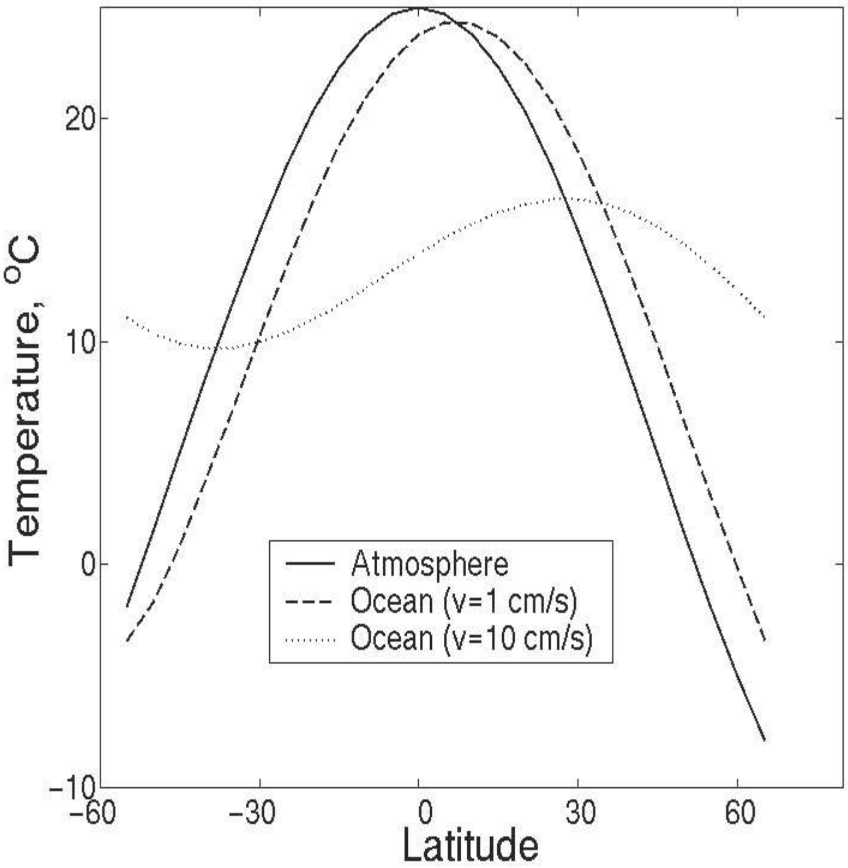

Fig 8: Analytical atmospheric and oceanic temperature profiles of the slab model. The solid line shows the fixed atmospheric cosine function. The dashed and dotted lines are the solutions of eq. (18) for the two velocities, $v = 1cm/s$ and $v = 10cm/s$. The other parameter choices were, T_m=278 K, T_o=20 K, λ=50 Wm$^{-2}K^{-1}$, ρ=1000 Kgm^{-3}, C_p=4000 JKg$^{-1}K^{-1}$, H= 1000 m. Increasing velocities flatten the oceanic temperature profile and shift its peaks northward.

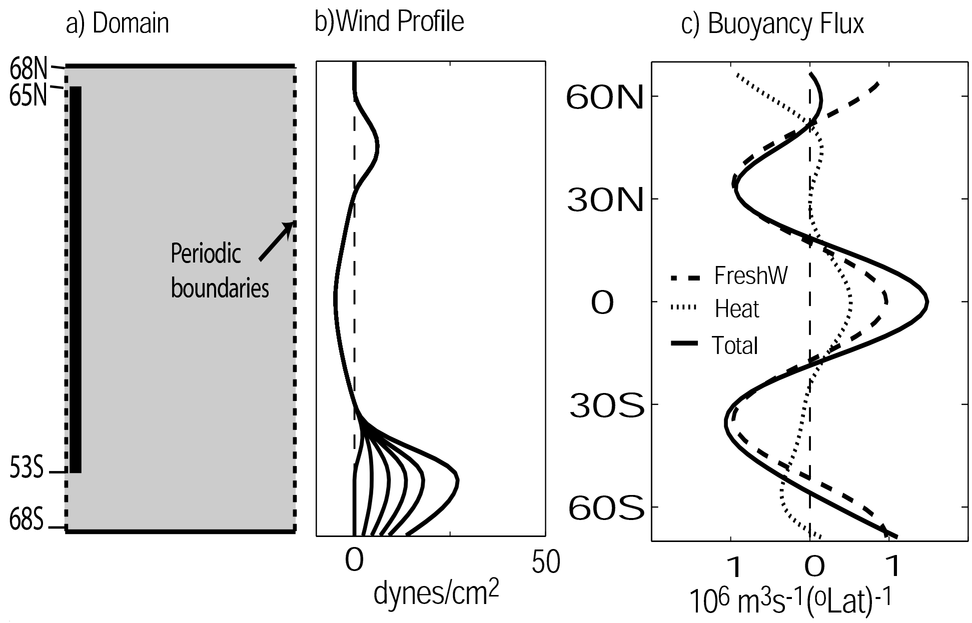

Fig 9: Description of the numerical model. The basin extends from 68^oS to 68^oN and is periodic in the zonal direction. An elongated island lies on the left between 53^oS and 65^oN. Winds are adapted from Hellerman and Rosenstein (b). South of the island, the winds are successively increased by a factor ranging from 0 to 3. An imposed buoyancy flux at the surface is converted to a mass flux (c). The freshwater flux (dashed line) is a fixed profile, while the heat flux (dotted line) depends on the upper layer thickness (see text for more details). The heat flux profile in (c) is for a wind amplification factor of 1 (Exp. 3). The combined buoyancy flux (solid line) shows a net buoyancy gain south of the island.

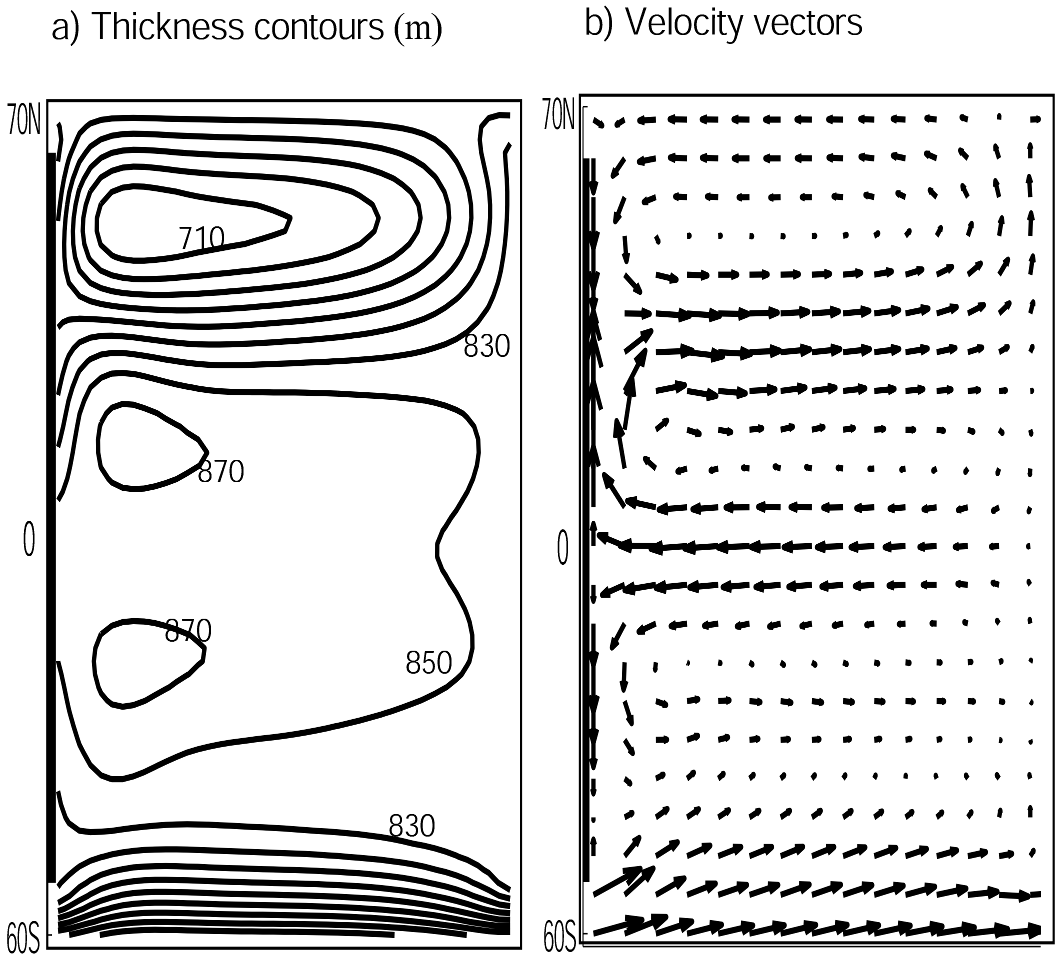

Fig 10: Upper layer thickness contour (a) and velocity vectors (b) for a wind amplification factor of 1. Two sub-tropical gyres sandwich the equator. A sub-polar gyre in the north is strengthened by sinking due to buoyancy loss. Strong zonal flows in the southernmost part of the ocean are omitted, as they distort the scale of the remaining basin.

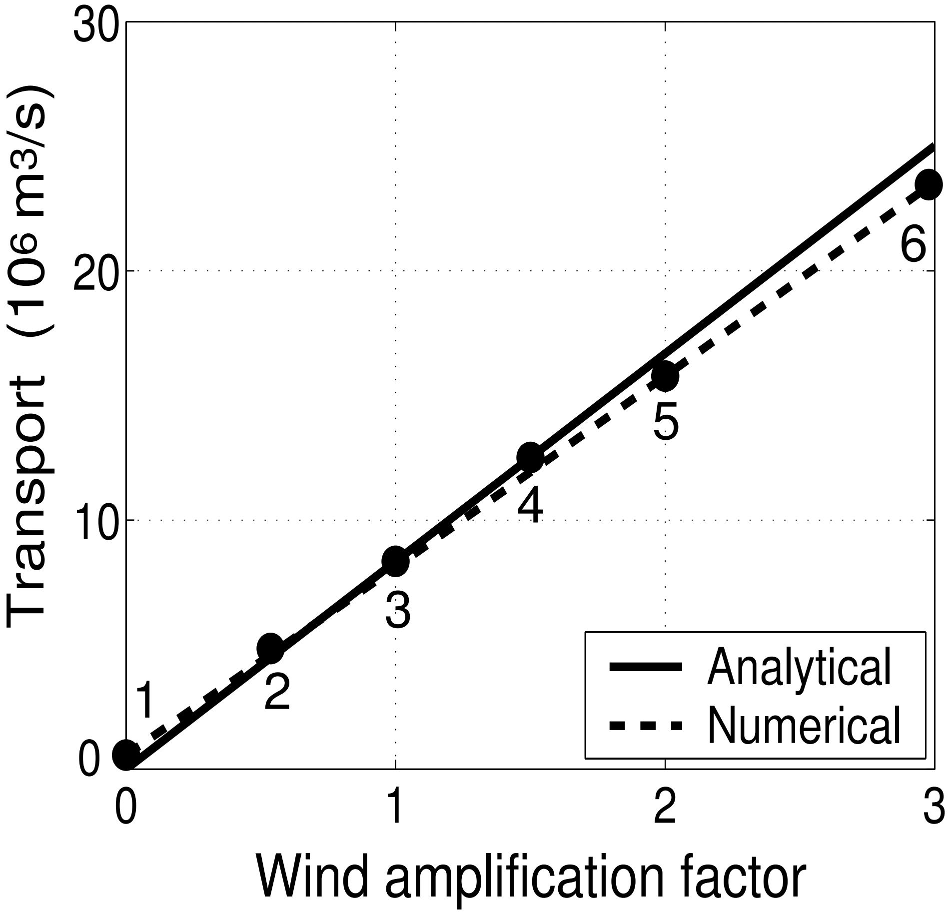

Fig 11: Transport across 55^{o}S, the latitude just south of the island (**Fig. 8**). The solid line is the analytical transport determined by the Belt Constraint (eq. 3). The dashed line shows the dependence of the numerical transport on the increased winds. Each bullet indicates a different run and is labeled by its experiment number (**Tab. 1**). The numerical flow agrees very closely with the Belt Constraint. The minute differences are due to lateral friction, linear drag and advection in the numerical model (**Fig. 12**).

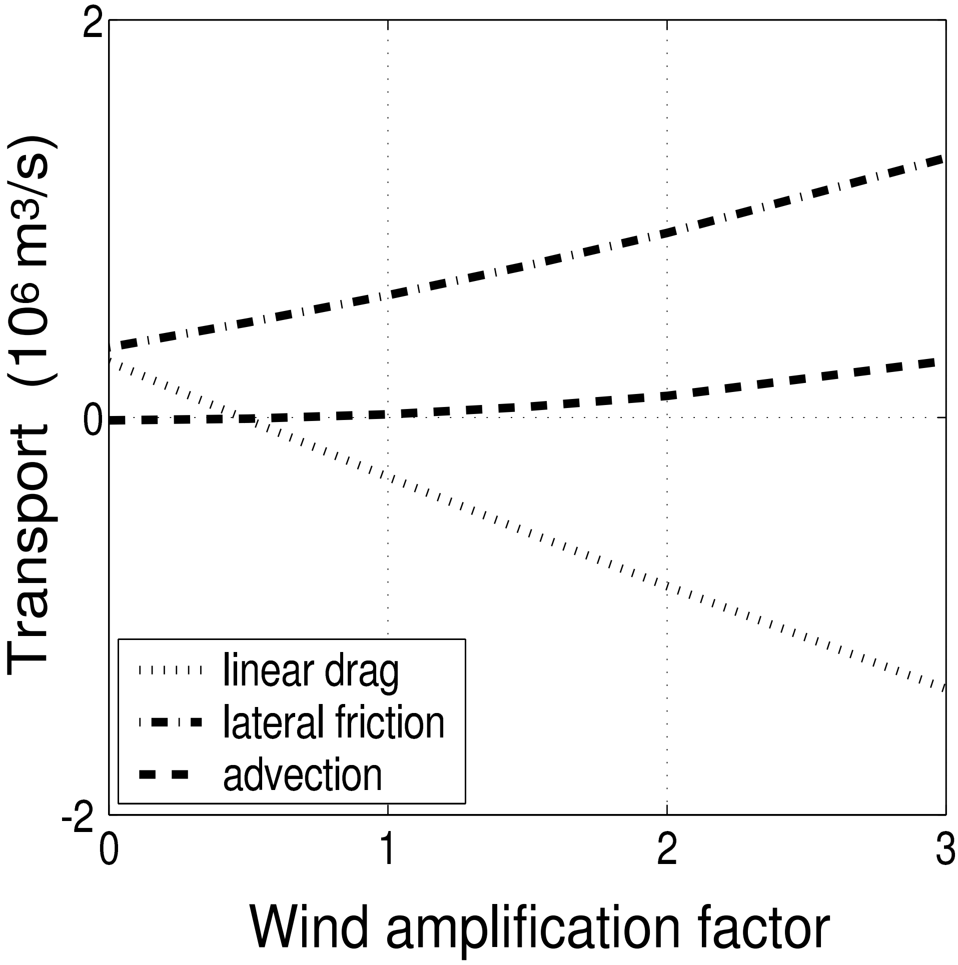

Fig 12: Terms neglected in the analytical derivation of the Belt Constraint transport. To compare the terms with the Belt Constraint results, units were converted to volume flux through a division by the coriolis parameter at 55^oS and then non-dimensionalized by dividing the terms by 13. Together the linear drag (dotted line), lateral friction (dash-dotted line) and advection (dashed line) account for the difference between the analytical and numerical solution in **Fig. 8**.